

# Energy transfer and locality in magnetohydrodynamic turbulence

Mahendra K. Verma<sup>1</sup> and Arvind Ayyer<sup>2</sup>

<sup>1</sup>*Department of Physics, Indian Institute of Technology, Kanpur – 208016, INDIA*

<sup>2</sup>*Department of Physics and Astronomy,  
Rutgers University, Piscataway, NJ, USA*

(Dated: April 15, 2004)

## Abstract

We analytically compute the strength of the nonlinear interactions, and the shell-to-shell energy transfer rates for magnetohydrodynamic (MHD) turbulence in the inertial range. We adopt a first-order field-theoretic technique for our calculation. The mode-to-mode energy transfer rates from velocity to velocity, velocity to magnetic, magnetic to velocity, and magnetic to magnetic fields are all forward and nonlocal in Fourier space. Regarding the shell-to-shell energy transfer, when magnetic and kinetic helicities are turned off, the energy transfer from velocity to velocity and magnetic to magnetic fields are forward and local. For kinetic-energy dominated MHD fluid, there is a preferential shell-to-shell energy transfer from kinetic to magnetic energy. The transfer is flipped for magnetic-energy dominated MHD fluid. This property of energy transfer in MHD turbulence is possibly the reason for equipartition of kinetic and magnetic energy in the asymptotic state of decaying MHD turbulence. When magnetic and kinetic helicities are turned on, the helical contributions are opposite to the corresponding nonhelical contributions.

PACS numbers: 47.65.+a, 52.30.Cv, 52.35.Ra

## I. INTRODUCTION

Energy transfers between wavenumber shells provide us with important insights into the dynamics of turbulence. Kolmogorov's fluid turbulence model is based on local energy transfer between wavenumber shells. There are several quantitative theories in fluid turbulence about the amount of energy transfer between neighbouring wavenumber shells. For examples, Kraichnan [1] showed that 35% of the energy flux comes from wavenumber triads where the smallest wave-number is greater than one-half of the middle wavenumber. This phenomenology has been verified using numerical and analytical methods [2, 3, 4, 5]. In this paper we will compute various shell-to-shell energy transfers in magnetohydrodynamic (MHD) turbulence using first-order field theory. We will investigate whether these transfers are local or not.

The interactions in MHD are through  $(\mathbf{u}(\mathbf{k}), \mathbf{u}(\mathbf{p}), \mathbf{u}(\mathbf{k} - \mathbf{p}))$  and  $(\mathbf{b}(\mathbf{k}), \mathbf{b}(\mathbf{p}), \mathbf{b}(\mathbf{k} - \mathbf{p}))$  triads, where  $(\mathbf{u}, \mathbf{b})$  are the velocity and magnetic fields respectively. The net effect is energy transfer from velocity/magnetic shell to velocity/magnetic shell. Kraichnan [1] gave a general formalism to compute the magnitudes of triad interactions and energy transfer between wavenumber shells using transfer function  $S(k|p, q)$  [6]. In this paper we will compute the magnitudes of nonlinear interactions, and the shell-to-shell energy transfer rates using a modified method called *mode-to-mode energy transfer rate*  $S(k|p|q)$ , which represents the energy transfer mode from  $\mathbf{p}$  to mode  $\mathbf{k}$ , with mode  $\mathbf{q}$  acting as a mediator. The new formalism is necessary for computing the shell-to-shell energy transfer because the earlier formalism suffers from ambiguity arising due to the third leg of the interaction (see Dar et al. [7, 8]). The calculation is done up to first-order in perturbation. We take Kolmogorov's spectrum for the energy spectrum as discussed in current numerical and analytical papers [9, 10, 11, 12, 13, 14].

In the present paper we compute the strength of triad interaction in the inertial range. MHD turbulence involves interactions between velocity and magnetic modes. Therefore, we compute interaction strengths between velocity to velocity, magnetic to magnetic, velocity to magnetic, and magnetic to velocity modes. After that we compute shell-to-shell energy transfer rates using these results. For our calculations, we have assumed that mean magnetic field and cross helicity are zero.

Pouquet et al. [15] first investigated whether interactions in MHD turbulence are local

or not. Their analysis is based on eddy-damped quasi-normal Markovian (EDQNM) calculation. They claimed that nonlocal interactions exist in MHD due to the mean magnetic field (Alfvén effect) and helicity. Unfortunately, in the current analytical work, we assume Kolmogorov’s spectrum for the velocity and magnetic fields, which limits our region of applicability to inertial range only. We will broadly compare our results with those of Pouquet et al.

The outline of the paper is as follows: In Sec. 2 we compute the strength of various types of triad interactions in MHD turbulence using mode-to-mode energy transfer rates  $S(k|p|q)$ . In Sec. 3 the shell-to-shell energy transfer rates are computed for nonhelical and helical MHD. The last section, Sec. 4, contains conclusions.

## II. TRIAD INTERACTIONS IN MHD TURBULENCE

We measure the strength of nonlinear interaction in a triad  $(\mathbf{k}', \mathbf{p}, \mathbf{q})$  participating in MHD turbulence using *mode-to-mode energy transfer rates* ( $S^{YX}(\mathbf{k}'|\mathbf{p}|\mathbf{q})$ ) that represents energy transfer rates from mode  $\mathbf{p}$  of field  $X$  to mode  $\mathbf{k}$  of field  $Y$ , with mode  $\mathbf{q}$  acting as a mediator. Note that  $\mathbf{k}' + \mathbf{p} + \mathbf{q} = 0$ . Dar et al.’s [7, 8] gave the following formulas for these quantities

$$\begin{aligned} S^{uu}(\mathbf{k}'|\mathbf{p}|\mathbf{q}) &= -\Im([\mathbf{k}' \cdot \mathbf{u}(\mathbf{q})][\mathbf{u}(\mathbf{k}') \cdot \mathbf{u}(\mathbf{p})]), \\ S^{bb}(\mathbf{k}'|\mathbf{p}|\mathbf{q}) &= -\Im([\mathbf{k}' \cdot \mathbf{u}(\mathbf{q})][\mathbf{b}(\mathbf{k}') \cdot \mathbf{b}(\mathbf{p})]), \\ S^{ub}(\mathbf{k}'|\mathbf{p}|\mathbf{q}) &= \Im([\mathbf{k}' \cdot \mathbf{b}(\mathbf{q})][\mathbf{u}(\mathbf{k}') \cdot \mathbf{b}(\mathbf{p})]), \\ S^{bu}(\mathbf{k}'|\mathbf{p}|\mathbf{q}) &= \Im([\mathbf{k}' \cdot \mathbf{b}(\mathbf{q})][\mathbf{b}(\mathbf{k}') \cdot \mathbf{u}(\mathbf{p})]), \end{aligned}$$

where  $\Im$  represents the imaginary part of the argument. We compute the ensemble average of  $S$  using the standard field-theoretic technique [16, 17, 18]. We expand the  $\langle S^{YX}(\mathbf{k}'|\mathbf{p}|\mathbf{q}) \rangle$  to first order in perturbation (see Verma [8, 12, 19] for details). As typically followed in field-theoretic treatment of turbulence, the flow is assumed to be homogeneous and isotropic.

In field-theoretic calculation  $\mathbf{u}(\mathbf{k})$  and  $\mathbf{b}(\mathbf{k})$  are assumed to be quasi-gaussian as in EDQNM approximation. Under this approximation, the triple correlation  $\langle XXX \rangle$  is zero to zeroth order, but nonzero to first order. To first order  $\langle XXX \rangle$  is written in terms of  $\langle XXXX \rangle$ , which is replaced by its Gaussian value, a sum of products of second-order moment. Consequently, the ensemble average of  $S^{YX}$ ,  $\langle S^{YX} \rangle$ , is nonzero to the first order.

The Feynman diagrams for these terms are given in Verma [8, 19]. We write  $\langle S^{YX}(k'|p|q) \rangle$  below in terms of Green's functions and correlation functions:

$$\begin{aligned}
\langle S^{uu}(k'|p|q) \rangle = & \int_{-\infty}^t dt' (2\pi)^3 [T_1(k, p, q) G^{uu}(k, t-t') C^u(p, t, t') C^u(q, t, t') \\
& + T_1'(k, p, q) G^{uu}(k, t-t') \frac{H_K(p, t, t')}{p^2} \frac{H_K(q, t, t')}{q^2} \\
& + T_5(k, p, q) G^{uu}(p, t-t') C^u(k, t, t') C^u(q, t, t') \\
& + T_5'(k, p, q) G^{uu}(p, t-t') \frac{H_K(k, t, t')}{k^2} \frac{H_K(q, t, t')}{q^2} \\
& + T_9(k, p, q) G^{uu}(q, t-t') C^u(k, t, t') C^u(p, t, t') \\
& + T_9'(k, p, q) G^{uu}(q, t-t') \frac{H_K(k, t, t')}{k^2} \frac{H_K(p, t, t')}{p^2}] \delta(\mathbf{k}' + \mathbf{p} + \mathbf{q}) \quad (1)
\end{aligned}$$

$$\begin{aligned}
\langle S^{ub}(k'|p|q) \rangle = & - \int_{-\infty}^t dt' (2\pi)^3 [T_2(k, p, q) G^{uu}(k, t-t') C^b(p, t, t') C^b(q, t, t') \\
& + T_2'(k, p, q) G^{uu}(k, t-t') H_M(p, t, t') H_M(q, t, t') \\
& + T_7(k, p, q) G^{bb}(p, t-t') C^u(k, t, t') C^b(q, t, t') \\
& + T_7'(k, p, q) G^{bb}(p, t-t') \frac{H_K(k, t, t')}{k^2} H_M(q, t, t') \\
& + T_{11}(k, p, q) G^{uu}(q, t-t') C^u(k, t, t') C^b(p, t, t') \\
& + T_{11}'(k, p, q) G^{uu}(q, t-t') \frac{H_K(k, t, t')}{k^2} H_M(p, t, t')] \delta(\mathbf{k}' + \mathbf{p} + \mathbf{q}) \quad (2)
\end{aligned}$$

$$\begin{aligned}
\langle S^{bu}(k'|p|q) \rangle = & - \int_{-\infty}^t dt' (2\pi)^3 [T_3(k, p, q) G^{bb}(k, t-t') C^u(p, t, t') C^b(q, t, t') \\
& + T_3'(k, p, q) G^{bb}(k, t-t') \frac{H_K(p, t, t')}{p^2} H_M(q, t, t') \\
& + T_6(k, p, q) G^{uu}(p, t-t') C^b(k, t, t') C^b(q, t, t') \\
& + T_6'(k, p, q) G^{uu}(p, t-t') H_M(k, t, t') H_M(q, t, t') \\
& + T_{12}(k, p, q) G^{bb}(q, t-t') C^b(k, t, t') C^u(p, t, t') \\
& + T_{12}'(k, p, q) G^{bb}(q, t-t') H_M(k, t, t') \frac{H_K(p, t, t')}{p^2}] \delta(\mathbf{k}' + \mathbf{p} + \mathbf{q}) \quad (3)
\end{aligned}$$

$$\begin{aligned}
\langle S^{bb}(k'|p|q) \rangle &= \int_{-\infty}^t dt' (2\pi)^3 [T_4(k, p, q) G^{bb}(k, t-t') C^b(p, t, t') C^u(q, t, t') \\
&+ T_4'(k, p, q) G^{bb}(k, t-t') H_M(p, t, t') \frac{H_K(q, t, t')}{q^2} \\
&+ T_8(k, p, q) G^{bb}(p, t-t') C^b(k, t, t') C^u(q, t, t') \\
&+ T_8'(k, p, q) G^{bb}(p, t-t') H_M(k, t, t') \frac{H_K(q, t, t')}{q^2} \\
&+ T_{10}(k, p, q) G^{uu}(q, t-t') C^b(k, t, t') C^b(p, t, t') \\
&+ T_{10}'(k, p, q) G^{uu}(q, t-t') H_M(k, t, t') H_M(p, t, t')] \delta(\mathbf{k}' + \mathbf{p} + \mathbf{q}) \quad (4)
\end{aligned}$$

where  $C^{u,b}(k, t, t')$  are the kinetic and magnetic spectra respectively,  $H_{K,M}(k, t, t')$  are the kinetic and magnetic helicities respectively,  $G^{uu,bb}$  are the kinetic and magnetic Green's function respectively, and  $T_i(k, p, q)$  are functions of wavevectors  $k, p$ , and  $q$  given in Verma [8, 19].

Green's functions can be written in terms of "effective" or "renormalized" viscosity  $\nu(k)$  and resistivity  $\eta(k)$  as

$$\begin{aligned}
G^{uu,bb}(k, t-t') &= \theta(t-t') \exp(-[\nu(k), \eta(k)]k^2(t-t')), \\
[\nu, \eta](k) &= (K^u)^{1/2} \Pi^{1/3} k^{-4/3} [\nu^*, \eta^*],
\end{aligned}$$

where the parameters  $\nu^*$  and  $\eta^*$  are renormalized parameters,  $K^u$  is Kolmogorov's constant for MHD turbulence, and  $\Pi$  is the total energy flux. The relaxation time for  $C^{uu}(k, t, t')$ ,  $H_K(k, t, t')$  [ $C^{bb}(k, t, t')$ ,  $H_M(k, t, t')$ ] is assumed to be the same as that of  $G^{uu}(k, t, t')$  [ $G^{bb}(k, t, t')$ ], and The equal-time correlation functions  $C^{uu}(k, t, t)$  and  $C^{bb}(k, t, t)$  are assumed to follow Kolmogorov's 5/3 powerlaw:

$$\begin{aligned}
C^{uu,bb}(k, t, t') &= \theta(t-t') \exp(-[\nu(k), \eta(k)]k^2(t-t')) C^{uu,bb}(k, t, t), \\
C^{uu,bb}(k, t, t) &= \frac{2(2\pi)^d}{S_d(d-1)} k^{-(d-1)} E^{u,b}(k),
\end{aligned}$$

with

$$\begin{aligned}
E^u(k) &= K^u \Pi^{2/3} k^{-5/3}; \quad E^b(k) = E^u(k)/r_A, \\
H_K(k) &= r_K k E^u(k); \quad H_M(k) = r_M E^b(k)/k,
\end{aligned}$$

where  $r_A$  is the Alfvén ratio. The above forms of Green's function and correlation functions are substituted in the expression of  $\langle S^{YX} \rangle$ , and the  $t'$  integral is performed. In this paper,

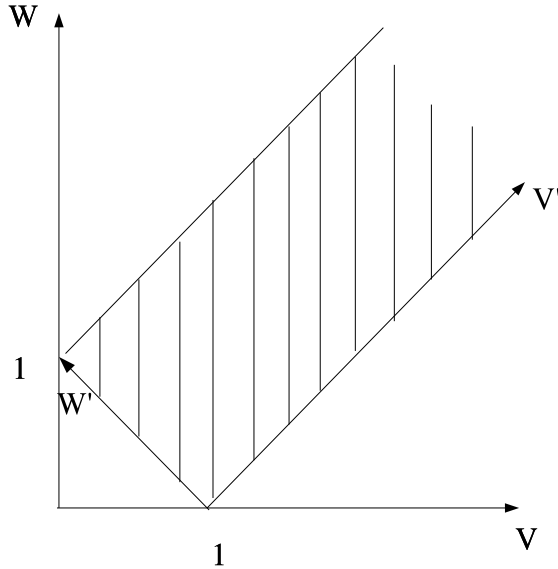


Figure 1: The interacting triad  $(\mathbf{k}, \mathbf{p}, \mathbf{q})/k = (1, v, w)$  under the condition  $\mathbf{k} = \mathbf{p} + \mathbf{q}$  can be represented as one point in the hatched region. The local wavenumbers are  $v \approx 1, w \approx 1$ .

we consider (a) nonhelical MHD ( $r_M = r_K = 0$  and different  $r_{AS}$ ), and (b) helical MHD ( $r_A = 1, r_K = 0.1, r_M = -0.1$ ). Our choice of  $r_K = 0.1$  (small positive) and  $r_M = -0.1$  (small negative) is one of the typical values taken in numerical simulations, or observed in astrophysical situations. For nonhelical MHD, the constants  $K^u, \nu^*, \eta^*$  are taken from Verma [13, 19]. For helical MHD, the constants are taken from Verma [20].

The physics in the inertial range is self-similar. Therefore, we analyze  $S^{YX}$  for triads  $(1, p/k, q/k) = (1, v, w)$ . Any triad can be represented as a point in the hatched region of Fig. 1 [17]. We substitute  $C(k)$ 's,  $\nu(k)$ , and  $\eta(k)$  in Eqs. (1-4), which yields  $\langle S^{YX}(k, p, q) \rangle$  in terms of  $(v, w)$ . As an example,

$$\frac{\langle S^{bb}(v, w) \rangle}{\Pi} = \left[ \frac{(K^u)^{3/2} (2\pi)^2}{k^6} \right] [F_{nonhelical}^{bb}(v, w) + F_{helical}^{bb}(v, w)] \quad (5)$$

with

$$F_{nonhelical}^{bb} = \frac{\frac{1}{r_A} t_4(v, w)(vw)^{-11/3} + \frac{1}{r_A} t_8(v, w)w^{-11/3} + \frac{1}{r_A^2} t_{10}(v, w)v^{-11/3}}{\eta^*(1 + v^{2/3}) + \nu^*w^{2/3}}, \quad (6)$$

$$F_{helical}^{bb} = \frac{\frac{r_M r_K}{r_A} t'_4(v, w)(vw)^{-11/3} + \frac{r_M r_K}{r_A} t'_8(v, w)w^{-11/3} + \frac{r_M r_M}{r_A^2} t'_{10}(v, w)v^{-11/3}}{\eta^*(1 + v^{2/3}) + \nu^*w^{2/3}}, \quad (7)$$

where  $t_i(v, w) = T_i(k, p, q)/k^2$ . The functions  $F_{nonhelical}^{YX}$  contains terms involving  $C(k)$ s, while the functions  $F_{helical}^{YX}$  contain terms with helicities. For  $F^{YX}$  refer to Verma [8, 20]. For convenience,  $S(v, w)$  are represented in terms of new variables  $(v', w')$  measured from the rotated axis shown in the figure 1. It is easy to show that  $v = 1 + (v' - w')/\sqrt{2}$ ,  $w = (v' + w')/\sqrt{2}$ .

In Fig. 2 we illustrate the contour plots of  $\langle F_{nonhelical}^{YX}(v, w) \rangle$  for nonhelical MHD with  $r_A = 1$ . Note that the function  $F_{nonhelical}^{YX}(v, w)$  represents the nonhelical energy transfer from mode  $p = v$  to mode  $k = 1$  with mode  $q = w$  acting as a mediator. The modes  $v$  in the white regions transfer energy to the mode  $k = 1$ , while the modes  $v$  in the dark region receive energy from mode  $k = 1$ . The energy transfer is from field  $X$  to field  $Y$ . Since  $F_{nonhelical}^{YX}(v, w)$  is large for small  $v$ , the nonlinear interactions in MHD turbulence are nonlocal in Fourier space, as in fluid turbulence [2, 5].

In Fig. 2  $F_{nonhelical}^{YX}(v, w)$  is positive for  $v < 1$  or  $v' < w'$ , and negative for  $v > 1$  or  $v' > w'$ , therefore we can deduce that nonhelical  $u$ -to- $u$  ( $F_{nonhelical}^{uu}$ ) and  $b$ -to- $b$  ( $F_{nonhelical}^{bb}$ ) energy transfers are forward. Note that  $F_{nonhelical}^{uu}(v = 1, w = 1) = F_{nonhelical}^{bb}(v = 1, w = 1) = 0$ . For  $d = 3$ , this trend is seen for all  $r_A$ .

For  $r_A > 1$ , we find that  $F_{nonhelical}^{bu}(v = 1, w = 1) > 0$  and  $F_{nonhelical}^{ub}(v = 1, w = 1) < 0$ , implying that for  $r_A > 1$  in  $(1, 1, 1)$  triad, energy is transferred from  $u$  to  $b$ . The transfer is reversed when  $r_A < 1$ . To get further insight into  $u$ -to- $b$  transfer, in Fig. 3 we plot  $F_{nonhelical}^{ub}(v', w') - F_{nonhelical}^{bu}(v', w')$  for three different  $r_A$ s:  $r_A = 0.5, 1, 2$ .

Fig. 3(a) ( $r_A = 0.5$ ) illustrates that  $F_{nonhelical}^{ub}(v', w') - F_{nonhelical}^{bu}(v', w')$  is positive for significant region with  $v < 1$ . That is, in magnetically dominated turbulence,  $b$ -to- $u$  forward energy transfer is more significant than  $u$ -to- $b$  forward energy transfer. The trend is reversed for  $r_A = 2$ , which is in the kinetic-energy dominated regime. The transition takes place around  $r_A = 1$ . These observations appear to indicate that for  $r_A > 1$ , energy transfer is dominantly from  $u$  to  $b$ , and the direction of energy transfer is reversed for  $r_A < 1$ .

We have varied space dimensionality  $d$  and studied the nature of  $F_{nonhelical}^{YX}$ . For  $d \geq 3$ ,

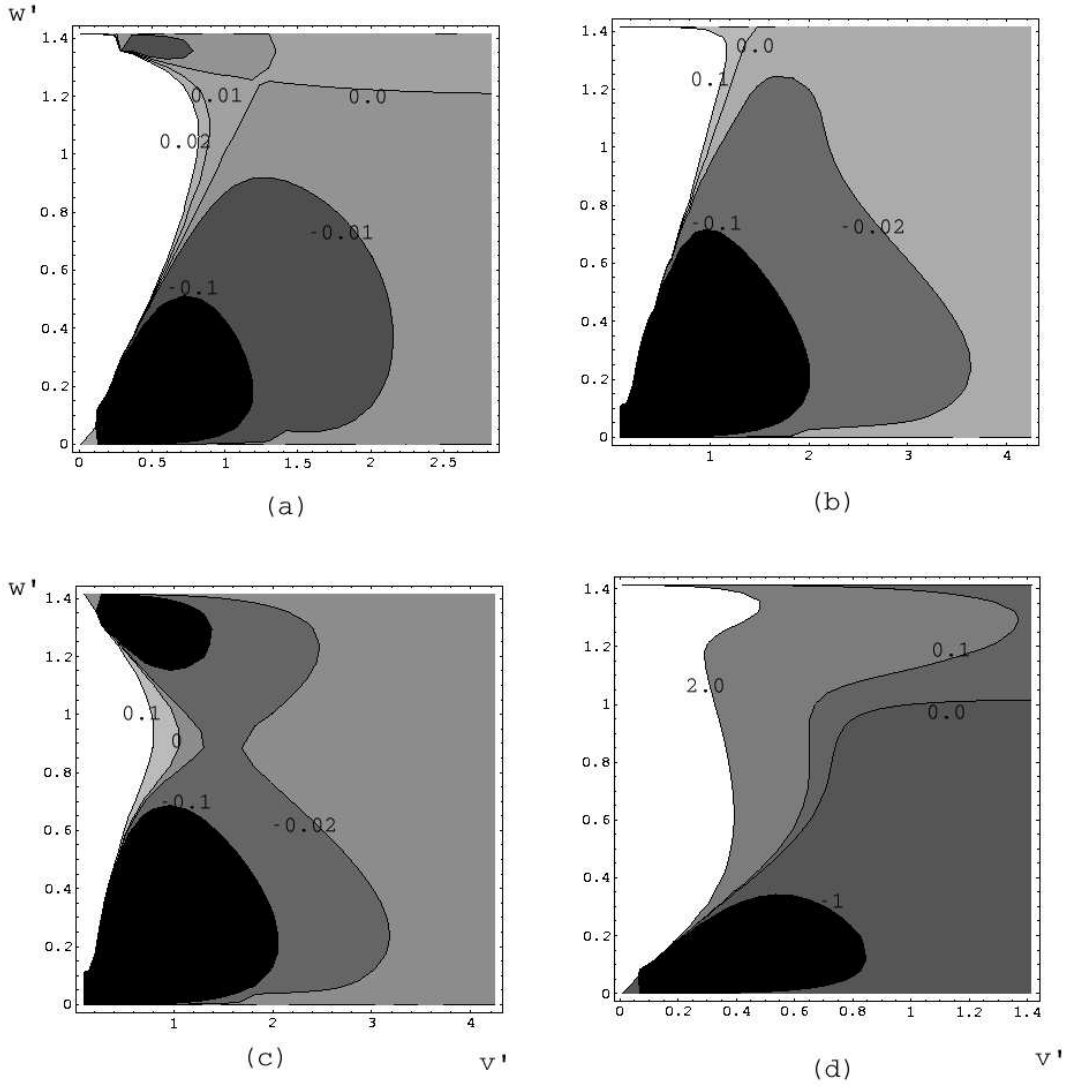


Figure 2: Contour plots of  $F_{nonhelical}^{YX}(v', w')$  computed for  $r_A = 1$ : (a)  $F_{nonhelical}^{uu}$  (b)  $F_{nonhelical}^{bb}$  (c)  $F_{nonhelical}^{ub}$  (d)  $F_{nonhelical}^{bu}$ .

the nature of  $F_{nonhelical}^{YX}$  are somewhat similar to that of  $d = 3$ . However, for large  $d$ , all  $F_{nonhelical}^{YX}$  are equal to each other. Also,  $F_{nonhelical}^{YX} > 0$  for all  $v < 1$ , and  $F_{nonhelical}^{YX} < 0$  for all  $v > 1$ . Refer to Fig. 4 For an illustration.

The nature of  $F_{nonhelical}^{YX}$  is quite different near  $d$  near 2.2. See Fig. 5 for an illustration. Here both  $S^{uu}$  and  $S^{ub}$  are negative for small  $v$  ( $v' \approx 0, w' \rightarrow \sqrt{2}$ ; top-left corner of  $v' - w'$  diagrams), indicating inverse energy transfer for  $u$ -to- $u$  and  $b$ -to- $u$  transfer. However,  $S^{bu}$  and  $S^{bb}$  are positive for small  $v$ . These results are consistent with the results obtained

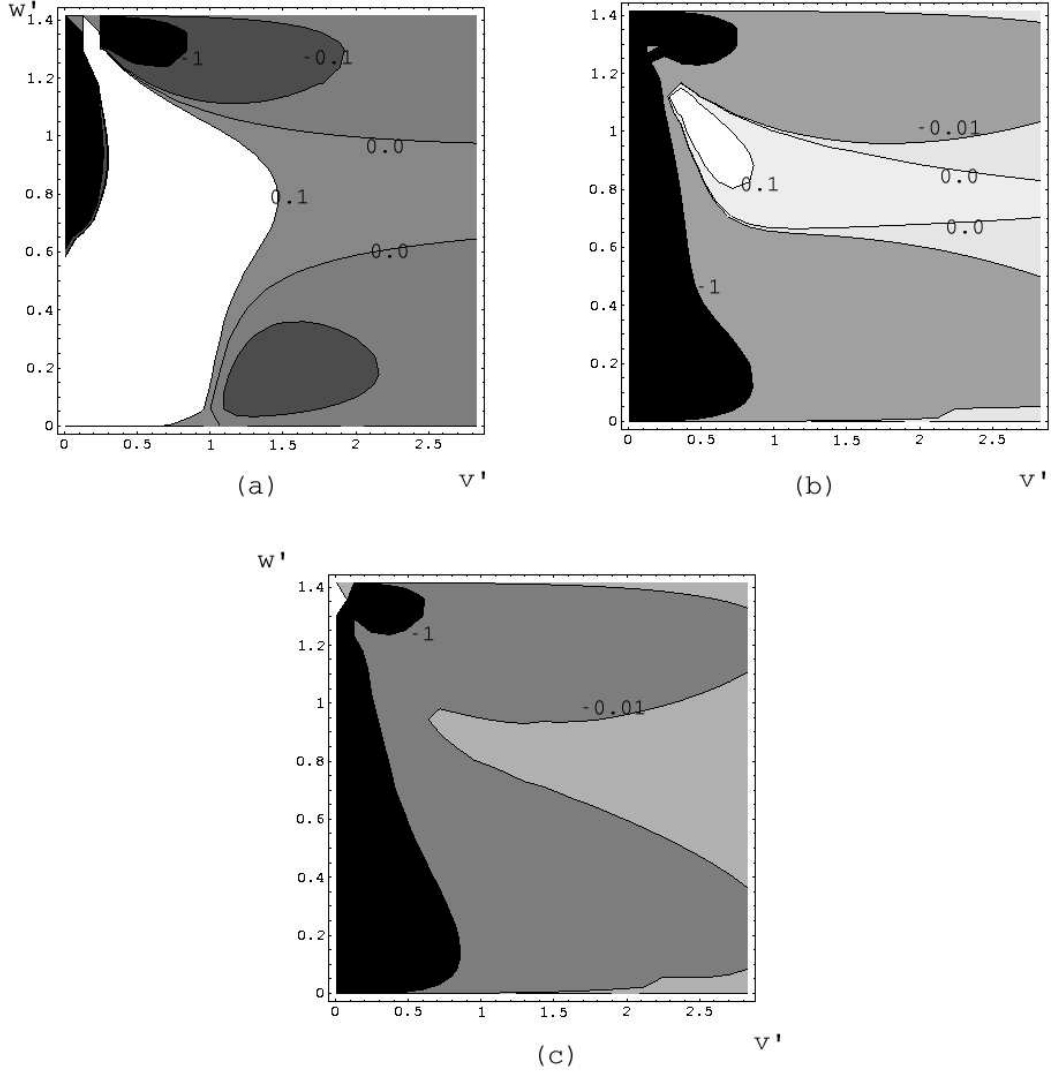


Figure 3: Contour plots of  $F_{nonhelical}^{ub}(v', w') - F_{nonhelical}^{bu}(v', w')$  for (a)  $r_A = 0.5$ , (b)  $r_A = 1$ , (c)  $r_A = 2$ .

earlier using renormalized group analysis of viscosity and resistivity [13] ( $\nu^{uu*}, \eta^{bu*} < 0$ ;  $\nu^{ub*}, \eta^{bb*} > 0$ ), and flux analysis [8, 19] where  $\Pi_{u>}^{u<}, \Pi_{u>}^{b<} < 0$ , and  $\Pi_{b>}^{u<}, \Pi_{b>}^{b<} > 0$ .

The mode-to-mode energy transfer gets contribution from the helical terms, as evident from Eq. (5). In Fig. 6 we illustrate the strength of helical part  $F_{helical}^{bb}(v', w')$  when  $r_A = 1, r_K = 0.1, r_M = -0.1$ .

The function  $F_{helical}^{uu}$ ,  $F_{helical}^{bb}$ , and  $F_{helical}^{ub}$  are negative for  $v < 1$ , indicating backward transfer of energy (from  $k = 1$  to  $p < 1$ ), but  $F_{helical}^{bu}$  has somewhat complex behaviour.

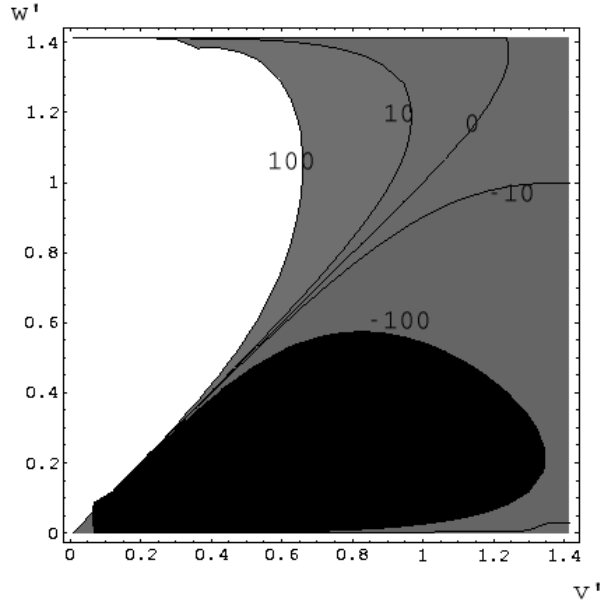


Figure 4: Contour plot of  $F_{nonhelical}^{ub}(v', w')$  for  $d = 100$ . All  $F_{nonhelical}^{YX}(v', w')$  are roughly the same.

$F_{helical}^{HM}$  is positive for  $v < 1$ , hence we expect the magnetic helicity to be transferred from small wavenumbers to large wavenumbers. Since  $r_M < 0$ , the magnetic helicity flux will be positive, a result consistent with the inverse cascade of magnetic helicity [20].

In the next section we will compute the shell-to-shell energy transfer in MHD turbulence using  $S^{YX}(k|p|q)$ .

### III. CALCULATION OF THE SHELL-TO-SHELL ENERGY TRANSFER

In this section we will compute the shell-to-shell energy transfer in MHD turbulence using as field-theoretic method. The energy transfer rates from  $m$ -th shell of field  $X$  to  $n$ -th shell of field  $Y$  is

$$T_{nm}^{YX} = \sum_{\mathbf{k}' \in n} \sum_{\mathbf{p} \in m} \langle S^{YX}(\mathbf{k}'|\mathbf{p}|\mathbf{q}) \rangle.$$

The  $\mathbf{p}$ -sum is over  $m$ -th shell, and the  $\mathbf{k}'$ -sum is over  $n$ -th shell.

The shells are binned logarithmically with the  $n$ -th shell being  $(k_0 s^{n-1}, k_0 s^n)$ . We nondi-

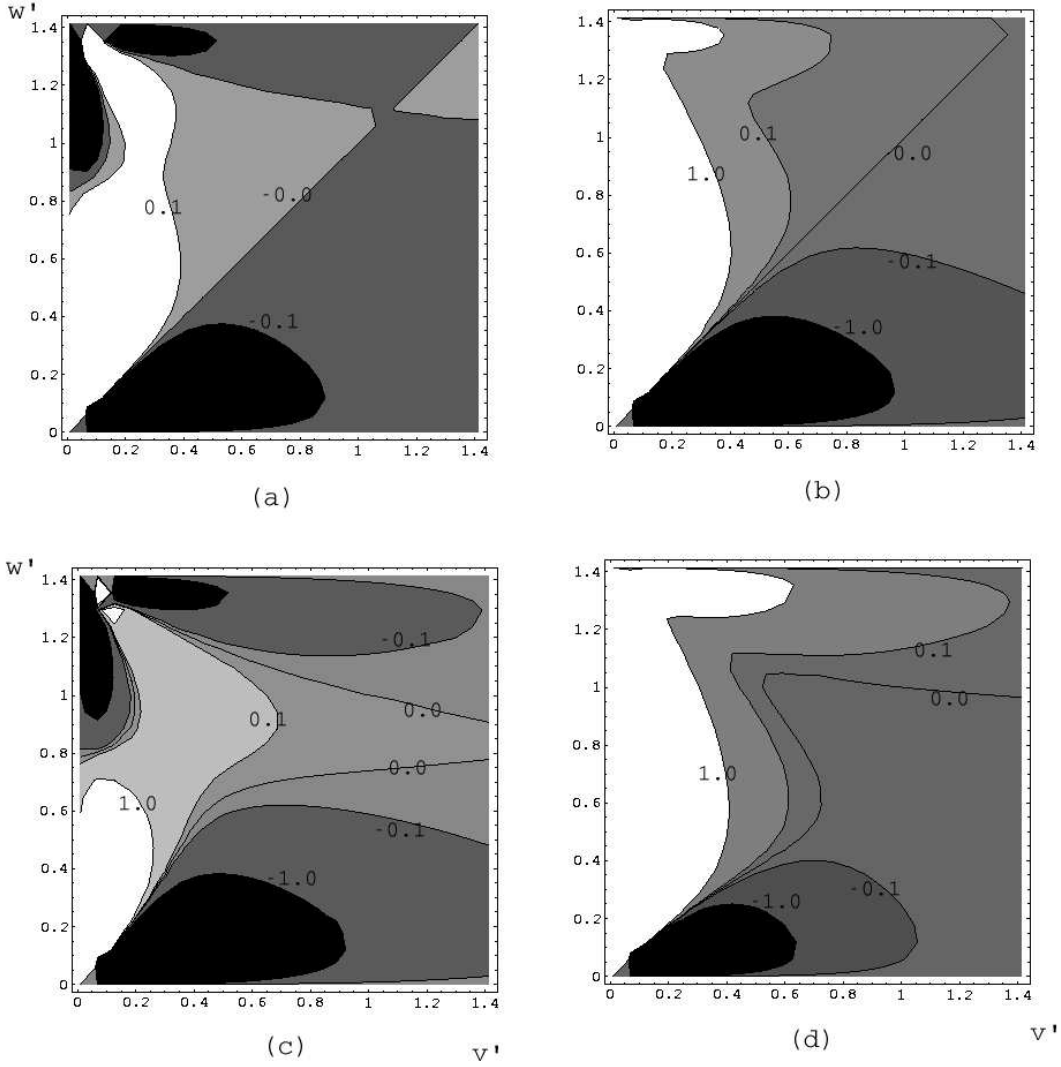


Figure 5: Contour plots of  $S^{YX}(v', w')$  for  $d = 2.2$ : (a)  $F_{nonhelical}^{uu}$  (b)  $F_{nonhelical}^{bb}$  (c)  $F_{nonhelical}^{ub}$  (d)  $F_{nonhelical}^{bu}$ .

mensionalize the equations using the transformation [17]

$$k = \frac{a}{u}; \quad p = \frac{a}{u}v; \quad q = \frac{a}{u}w, \quad (8)$$

where  $a = k_0 s^{n-1}$ . The resulting equation is

$$\frac{T_{nm}^{YX}}{\Pi} = K_u^{3/2} \frac{4S_{d-1}}{(d-1)^2 S_d} \int_{s^{-1}}^1 \frac{du}{u} \int_{us^{m-n}}^{us^{m-n+1}} dv \int_{|1-v|}^{1+v} dw (vw)^{d-2} (\sin \alpha)^{d-3} [F_{nonhelical}^{YX}(v, w) + F_{helical}^{YX}(v, w)], \quad (9)$$

where  $F_{nonhelical}^{bb}(v, w)$  and  $F_{helical}^{bb}(v, w)$  are given by Eqs. (6, 7). For  $F^{YX}$  refer to Verma

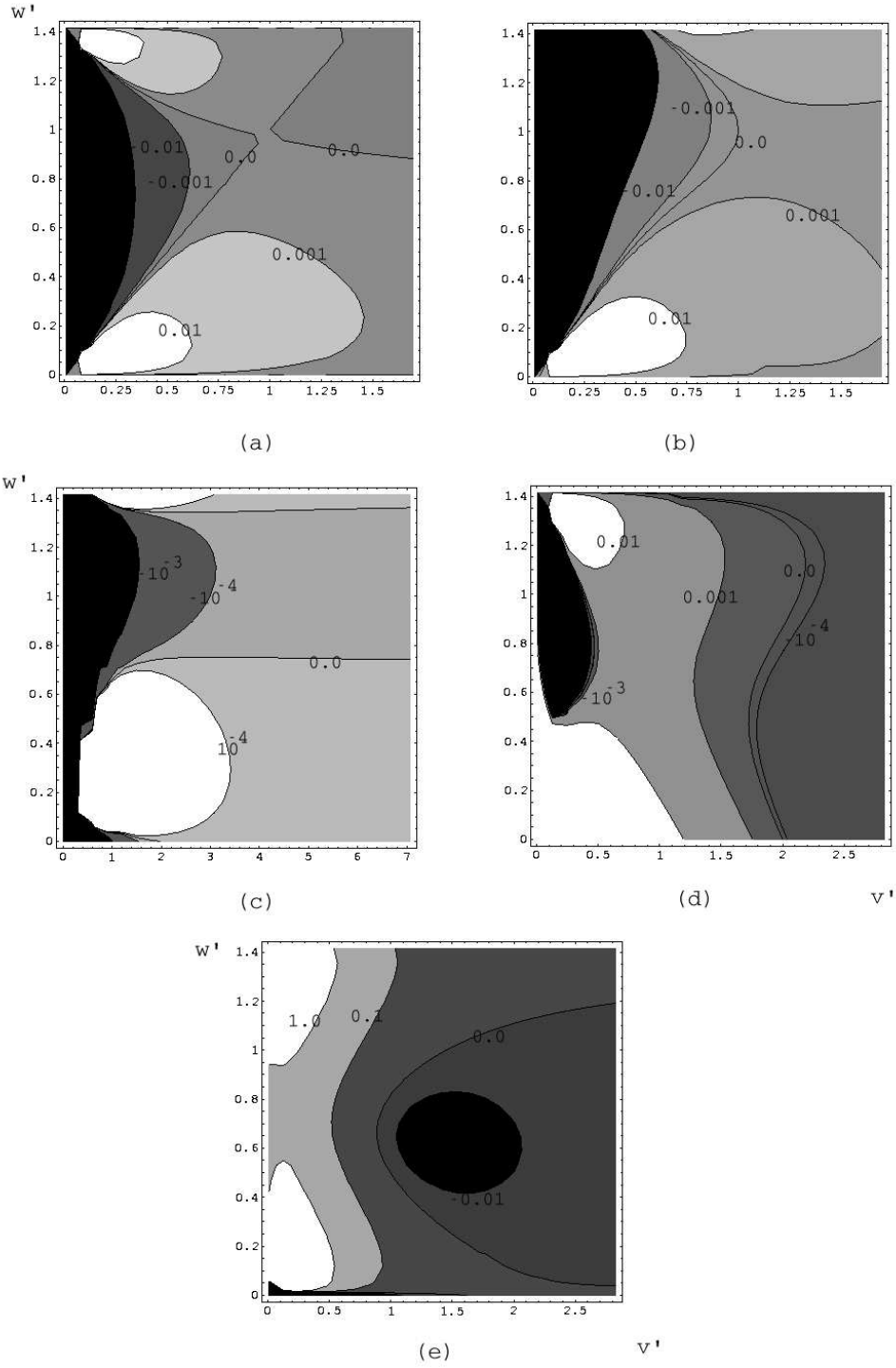


Figure 6: Contour plots of  $F_{helical}^{bb}(v', w')$  and  $F^{HM}(v', w')$  for  $r_K = 0.1, r_M = -0.1$  and  $r_A = 1$ .

(a)  $F_{helical}^{uu}$  (b)  $F_{helical}^{bb}$  (c)  $F_{helical}^{ub}$  (d)  $F_{helical}^{bu}$  (e)  $F_{helical}^{HM}$ .

[8, 20]. Note that the form of  $F^{YX}$  given in Eqs. (6, 7) are valid only inertial range, which is our region of focus. The renormalized parameters  $\nu^*$ ,  $\lambda^*$ , and Kolmogorov's constant  $K^u$  required to compute  $T_{nm}^{YX}/\Pi$  are taken Verma [8, 13, 19]. From Eq. (9) we can draw the following inferences:

1. The shell-to-shell energy transfer rate is a function of  $n-m$ , that is,  $\Phi_{nm} = \Phi_{(n-i)(m-i)}$ . Hence, the turbulent energy transfer rates in the inertial range are all self-similar. Note that this property holds only in the inertial range.
2.  $T_{nm}^{ub}/\Pi = -T_{mn}^{bu}/\Pi$ . Hence  $T_{nm}^{bu}/\Pi$  can be obtained from  $T_{mn}^{ub}/\Pi$  by inversion at the origin.
3.  $\Pi_{Y>}^{X<} = \sum_{n=m+1}^{\infty} (n-m)T_{nm}^{YX}$ .
4. Net energy gained by a  $u$ -shell from  $u$ -to- $u$  transfer is zero because of self similarity. However, a  $u$ -shell can gain or lose a net energy due to imbalance between  $u$ -to- $b$  and  $b$ -to- $u$  energy transfers. By definition, we can show that net energy gained by an inertial  $u$ -shell is

$$\sum_n (T_{nm}^{ub} - T_{nm}^{bu}) + T_{nn}^{ub}. \quad (10)$$

Similarly, net energy gained by a  $b$ -shell from  $b$ -to- $b$  transfer is zero. However, net energy gained by an inertial  $b$ -shell due to  $u$ -to- $b$  and  $b$ -to- $u$  transfers is

$$\sum_n (T_{nm}^{bu} - T_{nm}^{ub}) + T_{nn}^{bu}. \quad (11)$$

Now we compute the integrals of Eq. (9), and denote the nonhelical and helical parts by  $(T_{nm}^{YX})_{nonhelical}$  and  $(T_{nm}^{YX})_{helical}$  respectively. Their properties are described below.

1. *Nonhelical shell-to-shell energy transfer:*

We compute the nonhelical shell-to-shell energy transfer using  $F_{nonhelical}^{YX}$ . We have chosen  $s = 2^{1/4}$ . This study has been done for various values of Alfvén ratios. Fig. 7 contains plots of  $T_{nm}^{YX}/\Pi$  vs.  $n-m$  for four typical values of  $r_A = 0.5, 1, 5, 100$ . The numbers on the plots represent energy transfer rates from shell  $m$  to shells  $m+1, m+2, \dots$  in the right, and to shells  $m-1, m-2, \dots$  in the left. All the plots are to same scale. For  $r_A = 0.5$ ,

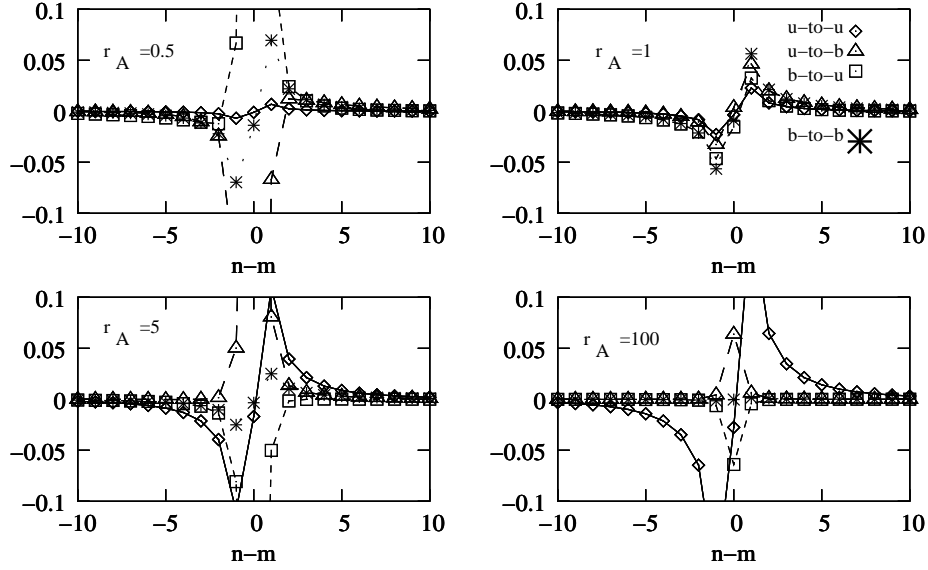


Figure 7: Theoretically calculated values of  $T_{nm}^{YX}/\Pi$  vs.  $n - m$  for zero helicities ( $\sigma_c = r_K = r_M = 0$ ) and Alfvén ratios  $r_A = 0.5, 1, 4, 100$ . For  $r_A = 0.5$ , the maxima of  $(T_{nm}^{ub})_{nonhelical}/\Pi$  and  $(T_{nm}^{bu})_{nonhelical}/\Pi$  are  $\pm 1.40$  respectively, out of scale of the plot. The corresponding values for  $r_A = 5$  are  $\mp 0.78$

the maxima of  $(T_{nm}^{ub})_{nonhelical}/\Pi$  and  $(T_{nm}^{bu})_{nonhelical}/\Pi$  occurs at  $m = n$ , and its values are  $\pm 1.40$  respectively. The corresponding values for  $r_A = 5$  are  $\mp 0.78$ . By observing the plots we find the following interesting patterns:

1.  $(T_{nm}^{uu})_{nonhelical}/\Pi$  is positive for  $n > m$ , and negative for  $n < m$ . Hence, a  $u$ -shell gains energy from smaller wavenumber  $u$ -shells, and loses energy to higher wavenumber  $u$ -shells, implying that the energy cascade is forward. Also, the absolute maximum occurs for  $n = m \pm 1$ , hence the energy transfer is local. For kinetic energy dominated regime,  $s = 2^{1/2}$  yields  $T_{nm}^{uu}/\Pi \approx 35\%$ , similar to Kraichnan's Test Mean Field model (TFM) predictions [1].
2.  $T_{nm}^{bb}/\Pi$  is positive for  $n > m$ , and negative for  $n < m$ , and maximum for  $n = m \pm 1$ . Hence magnetic to magnetic energy transfer is forward and local. This result is consistent with the forward magnetic-to-magnetic cascade ( $\Pi_{b>}^{b<} > 0$ ) [8, 19].

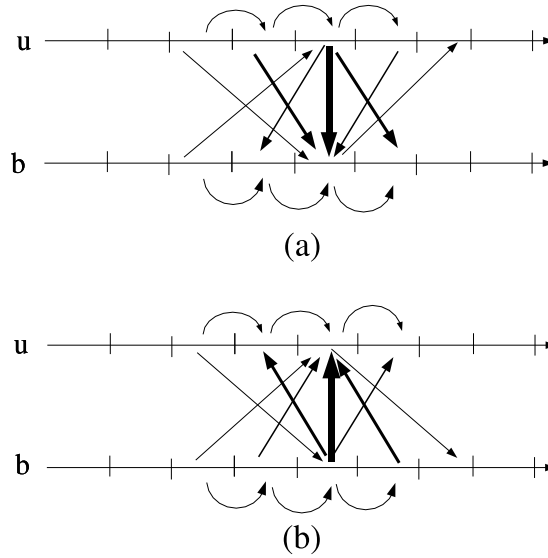


Figure 8: Schematic illustration of nonhelical  $T_{nm}^{YX}/\Pi$  in the inertial range for (a) kinetic-energy dominated regime, and (b) magnetic-energy dominated regime. In (a)  $T_{nm}^{bu}/\Pi$  is positive for  $n \geq m-1$ , and negative otherwise, while in (b)  $T_{nm}^{ub}/\Pi$  is positive for  $n \geq m-1$ , and negative otherwise.  $T_{nm}^{uu}$  and  $T_{nm}^{bb}$  is forward and local.

3. For  $r_A > 1$  (kinetic energy dominated), kinetic to magnetic energy transfer rate  $(T_{nm}^{bu})_{nonhelical}/\Pi$  is positive for  $n \geq m-1$ , and negative otherwise. These transfers have been illustrated in Fig. 8(a). Using Eq. (11) we find that each  $u$ -shell loses a net kinetic energy to  $b$ -shells, hence the turbulence is not steady. This phenomena is seen for all  $r_A > 1$ . The net energy transfer rate from a shell however decreases as we go toward  $r_A = 1$ .
4. For  $r_A = 0.5$  (magnetically dominated), magnetic to kinetic energy transfer rate  $(T_{nm}^{ub})_{nonhelical}/\Pi$  is positive for  $n \geq m-1$ , and negative otherwise (see Fig. 7). In addition, using Eq. (10) we find that each  $b$ -shell loses a net magnetic energy to  $u$ -shells, hence the turbulence cannot be steady. This phenomena is seen for all  $r_A < 1$ . The net energy transfer rate from a shell however decreases as we go toward  $r_A = 1$ .
5. The observations of (3) and (4) indicate that kinetic to magnetic or the reverse energy transfer rate almost vanishes near  $r_A = 1$ . *We believe that MHD turbulence evolves toward  $r_A \approx 1$  due to the above reasons.* For  $r_A \neq 1$ , MHD turbulence is not steady.

This result is same as Pouquet et al.'s prediction of equipartition of kinetic and magnetic energy using EDQNM calculation [15]. Note however that the steady-state value of  $r_A$  in numerical simulations and solar wind is around 0.5-0.6. The difference is probably because the realistic flows have more interactions than those discussed above, e. g., nonlocal coupling with forcing wavenumbers. Careful numerical simulations are required to clarify this issue.

6. When  $r_A$  is not close to 1 ( $r_A \leq 0.5$  or  $r_A > 5$ ),  $u$ -to- $b$  shell-to-shell transfer involves many neighbouring shells (see Fig. 7). This observation implies that  $u$ - $b$  energy transfer is somewhat nonlocal as predicted by Pouquet et al. [15].
7. We compute energy fluxes using  $T_{nm}^{YX}$ , and find them to be the same as that computed by Verma [8, 19]. Hence both the results, flux and shell-to-shell energy transfer rates, are consistent with each other.

After the above discussion on nonhelical MHD, we move to helical MHD.

## 2. Helical Contributions:

Now we present computation of  $(T_{nm}^{YX})_{helical}/\Pi$ , helical shell-to-shell energy transfer rates for helical MHD ( $H_M \neq 0, H_K \neq 0$ ) [20]. To simplify the equation, we consider only nonAlfvénic fluctuations ( $\sigma_c = 0$ ). We have chosen  $r_A = 1, r_K = 0.1, r_M = -0.1$ . These are one of the typical parameters chosen in numerical simulations. For the above choice of parameters, Kolmogorov's constant  $K^u = 0.78$  [20]. In Fig. 9 we have plotted  $(T_{nm}^{YX})_{helical}/\Pi$  vs  $n - m$ . Our results on helical shell-to-shell transfers are given below:

1. Comparison of Fig. 9 with Fig. 7 ( $r_A = 1$ ) shows that helical transfers are order-of-magnitude lower than the nonhelical ones for the parameters chosen here ( $r_A = 1, r_K = 0.1, r_M = -0.1$ ). For maximal helicity, the helical and nonhelical values become comparable.
2. All the helical contributions are negative for  $n > m$ , and positive for  $n < m$ . Hence, helical transfers are from larger wavenumbers to smaller wavenumbers. This is consistent with the inverse cascade of energy due to helical contributions, as discussed by Pouquet et al. [15, 20].

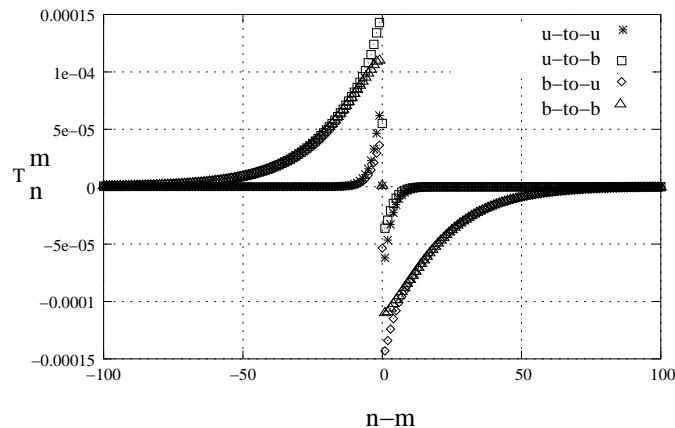


Figure 9: Theoretically calculated values of *helical contributions to*  $(T_{nm}^{YX})_{helical}/\Pi$  vs.  $n - m$  in helical MHD with  $r_A = 1, r_K = 0.1, r_M = -0.1$  and  $\sigma_c = 0$ .

3. We find that  $(T_{nm}^{ub})_{helical}$  and  $(T_{nm}^{bb})_{helical}$  is significantly positive for  $-50 < n - m \leq 0$ . This signals a nonlocal *b-to-b* and *u-to-b* inverse energy transfers. Hence, helicity induces nonlocal energy transfer between *b-to-b* and *u-to-b* wavenumber shells. This is in agreement with Pouquet et al.’s result [15] that “residual helicity” induces growth of large-scale magnetic field by nonlocal interactions.

In the next section we summarize our results.

#### IV. CONCLUSIONS

In this paper we computed the strength of nonlinear interactions and the shell-to-shell energy transfers in MHD turbulence using first-order field theoretic technique. The strength of nonlinear interactions is measured using mode-to-mode energy transfer between two modes. We find that the nonlinear interactions are nonlocal in Fourier space, i. e., interactions between distant wavenumber is large. All the nonhelical energy transfers *u-to-u*, *b-to-b*, *u-to-b*, *b-to-u* are forward, i. e., from smaller wavenumber modes to larger wavenumber modes. However, for  $r_A > 1$ , *u-to-b* energy transfer dominates *b-to-u* energy transfer. On the contrary, for  $r_A < 1$ , *b-to-u* energy transfer dominates *u-to-b* energy transfer. The helical energy transfers are backward, i. e., from large larger wavenumbers to smaller wavenumbers.

We have computed the shell-to-shell energy transfer rates using field-theoretic method. The contributions of nonhelical and helical terms have been calculated separately. We find that the nonhelical  $u$ -to- $u$  and  $b$ -to- $b$  shell-to-shell energy transfer is local as in fluid turbulence, i. e., most of energy from a wavenumber shell is transferred to neighbouring shells. Comparatively, nonhelical  $u$ -to- $b$  and  $b$ -to- $u$  energy transfers involves distant shells for  $r_A \gg 1$ , or  $r_A < 1$ . For  $r_A > 1$ , there is a preferential transfer of kinetic energy to magnetic energy; in fact, a  $u$ -shell loses a net amount of kinetic energy to  $b$ -shell. From this result we can conclude that kinetic-energy dominated MHD fluid cannot be in a steady state. For  $r_A < 1$ , the pattern of  $u$ -to- $b$  energy transfer is reversed, and there is a a net transfer of energy from magnetic to kinetic. This preferential energy transfer is minimum for  $r_A \approx 1$ . The above property of the shell-to-shell energy transfer is possibly the reason why all the decaying MHD turbulence evolve to approximate equipartition of kinetic and magnetic energy. The asymptotic state in real flows have  $r_A \approx 0.4 - 0.6$ , somewhat different than  $r_A = 1$  envisaged here. The difference may be due to the interactions not accounted for in our idealized calculation.

We find that helical shell-to-shell energy transfer is backward, that is from larger wavenumbers to smaller wavenumbers. For  $r_K = 0.1, r_M = -0.1$ , one of the typical values observed in numerical simulations, the helical shell-to-shell energy transfer is order-of-magnitude smaller than the nonhelical ones. However, for maximal helicity, the helical shell-to-shell energy transfer is comparable to the nonhelical ones.

To conclude, an application of field-theoretic techniques to turbulence yields interesting results regarding triad interactions and shell-to-shell energy transfers in MHD turbulence.

- 
- [1] R. H. Kraichnan, J. Fluid Mech. **47**, 525 (1971).
  - [2] J. A. Domaradzki and R. S. Rogallo, Phys. Fluids A **2**, 413 (1990).
  - [3] Y. Zhou, Phys. Fluids **5**, 1092 (1993).
  - [4] Y. Zhou and C. G. Speziale, Appl. Mech. Rev. **51**, 267 (1998).
  - [5] M. K. Verma, A. Ayyer, S. Kumar, and A. V. Chandra, Submitted to J. Fluid Mech. (2004).
  - [6] M. Lesieur, *Turbulence in Fluids - Stochastic and Numerical Modelling* (Kluwer Academic Publishers, Dordrecht, 1990).

- [7] G. Dar, M. K. Verma, and V. Eswaran, *Physica D* **157**, 207 (2001).
- [8] M. K. Verma, Submitted to *Phys. Rep.* (2004).
- [9] M. K. Verma, *Phys. Plasmas* **6**, 1455 (1999).
- [10] S. Sridhar and P. Goldreich, *Astrophys. J.* **432**, 612 (1994).
- [11] P. Goldreich and S. Sridhar, *Astrophys. J.* **438**, 763 (1995).
- [12] M. K. Verma, *Phys. Rev. E* **64**, 26305 (2001).
- [13] M. K. Verma, *Phys. Plasmas* **8**, 3945 (2001).
- [14] M. Hnatich, J. Honkonen, and M. Jurcisin, *Phys. Rev. E* **64**, 56411 (2001).
- [15] A. Pouquet, U. Frisch, and J. Léorat, *J. Fluid Mech.* **77**, 321 (1976).
- [16] R. H. Kraichnan, *Phys. Fluids* **8**, 1385 (1965).
- [17] D. C. Leslie, *Development in the Theory of Turbulence* (Oxford University Press, Clarendon, 1973).
- [18] W. D. McComb, *The Physics of Fluid Turbulence* (Oxford University Press, Clarendon, 1990).
- [19] M. K. Verma, *Pramana* **61**, 577 (2003).
- [20] M. K. Verma, *Pramana* **61**, 707 (2003).